Band Structure and Fermi Surface of Beryllium*

T. L. Loucks† and P. H. Cutler
Department of Physics, The Pennsylvania State University, University Park, Pennsylvania
(Received 23 August 1963)

Using a self-consistent potential, the energy eigenvalues along the symmetry edges, on the zone faces, and at the equivalent of 5184 general points in the first Brillouin zone were calculated for beryllium by expanding the conduction electron wave functions in a linear combination of 23 orthogonalized plane waves. From this the Fermi energy and density of states were calculated and the Fermi surface constructed. The density of states is in agreement with soft x-ray emission and absorption data and with the experimental low-temperature specific heat coefficient. The Fermi surface consists of three pieces: A region of unoccupied states in the first double zone which resembles a coronet, and two identical pockets of electrons in the second double zone similar in shape to a cigar with a triangular cross section. The de Haas-van Alphen frequencies in $1/H$ predicted from the Fermi surface are in good agreement with those measured experimentally.

INTRODUCTION

THE band structure and other electronic properties of beryllium were first calculated by Herring and Hill[1] (HH) in the initial application of the orthogonalized plane wave (OPW) method. Their pioneering effort has served as the basis for many more subsequent energy band calculations using this method.[2–6] Since techniques for investigating the Fermi surface directly have only been developed within the last decade, a test of their work has generally been restricted to the comparison of the density-of-states curve for the conduction electrons with experiments dependent on this quantity. For example, the soft x-ray spectroscopy of beryllium has been found to be in qualitative agreement with the work of HH. Although they predicted a value for the density of states at the Fermi energy which was much lower than the free-electron value, it agreed quite well with the experimental values of the low-temperature electronic specific heat coefficient determined by Hill and Smith in 1953.[7]

A more critical test, however, of their energy bands has only recently become available. Watts[8] proposed a Fermi surface for beryllium based on de Haas–van Alphen measurements. The Fermi surface based on HH's band structure agrees qualitatively with these experiments only if one arbitrarily choses a Fermi energy different from the one they propose. The present work on beryllium had been started before the experiments of Watts pointed out this disagreement between the theoretical calculation and experiment. In the following paragraphs we indicate the ways the calculations needed to be improved.

A first step toward improving the calculations was in the construction of the crystal potential. Aside from the usual Coulombic terms the following have now been included: correlation between ion-core electrons, exchange and correlation between conduction electrons and a correction for deviation from spherical symmetry around the core. Furthermore, the potential is felt to be the most self-consistent yet produced. For the conduction electrons single OPW wave functions (solved using the potential itself) were used in all the appropriate terms contributing to the potential. The core-state wave functions occurring in the potential terms were taken to be the ground-state solutions of the crystal potential itself. The potential was thus constructed by a series of four iterations until the conduction and core wave functions used to construct the potential were in fact solutions to it.

Furthermore, enough general points (equivalent to 5184) were computed in the first Brillouin zone (BZ) to define more accurately both the density of states and the Fermi energy. At all of these points a 23×23 secular determinant was solved for the lowest lying eigenvalues. The energy bands along all the symmetry edges and the zone faces were also determined in this manner. This information made possible a more exact determination of the Fermi energy, density of states, and the Fermi surface.

THEORY

Hexagonal Close-Packed Lattice

In dealing with the direct and reciprocal lattices it is convenient to use the following representations:

$$(a,b,c)=a\mathbf{t}_1+b\mathbf{t}_2+c\mathbf{t}_3$$
$$[a,b,c]=a\mathbf{K}_1+b\mathbf{K}_2+c\mathbf{K}_3.$$

The $\mathbf{t}$ basis defines the unit cell in the direct lattice such that

$$\mathbf{t}_1=c\hat{k},\quad \mathbf{t}_2=a\hat{\imath},\quad \mathbf{t}_3=a(-\tfrac{1}{2}\hat{\imath}+\tfrac{1}{2}\sqrt{3}\hat{\jmath}),$$

* Work supported by the U. S. Air Force Office of Scientific Research, Grant Numbers AF-AFOSR-61-100 and AF-AFOSR-213-63.

† This paper is based on a dissertation submitted by T. L. Loucks in partial fulfillment of the requirements for the Ph.D. degree in Physics at The Pennsylvania State University.

[1] C. Herring and A. G. Hill, Phys. Rev. **58**, 132 (1940).
[2] R. H. Parmenter, Phys. Rev. **86**, 552 (1952).
[3] F. Herman, Phys. Rev. **93**, 1214 (1954).
[4] T. O. Woodruff, in *Solid State Physics*, edited by F. Seitz and D. Turnbull (Academic Press Inc., New York, 1957), Vol. 4, p. 367.
[5] V. Heine, Proc. Roy. Soc. (London), **A240**, 340, 361 (1957).
[6] L. M. Falicov, Phil. Trans. Roy. Soc. (London) **A255**, 55 (1962).
[7] R. W. Hill and P. L. Smith, Phil. Mag. **44**, 636 (1953).
[8] B. R. Watts, Phys. Letters **3**, 284 (1963).

where $\hat{\imath}$, $\hat{\jmath}$, and $\hat{k}$ are unit orthogonal vectors (see Fig. 1). c and a are the lattice parameters; the values used in this calculation are given by Schwarzenberger[9]:

$$c=6.77152, \quad a=4.32109.$$

The units are defined by $\hbar=1$, $e^2=2$ and $m=\frac{1}{2}$; energy in rydbergs and length in units of the Bohr radius. The unit cell contains two atoms (4 conduction electrons) located at (0,0,0) and $(\frac{1}{2},\frac{1}{3},\frac{2}{3})$. The volume of the unit cell is

$$\Omega_0=\mathbf{t}_1\cdot\mathbf{t}_2\times\mathbf{t}_3=a^2c\sqrt{3}/2=109.5.$$

The atomic radius, $r_s=2.37$, is defined by

$$\tfrac{4}{3}\pi r_s^3=\tfrac{1}{2}\Omega_0.$$

The $\mathbf{K}$ basis defines the reciprocal space lattice:

$$\mathbf{K}_i\cdot\mathbf{t}_j=2\pi\delta_{ij} \quad i,j=1,2,3.$$

Thus,

$$\mathbf{K}_1=(2\pi/c)\hat{k},$$
$$\mathbf{K}_2=(2\pi/a\sqrt{3})(\hat{\jmath}+\sqrt{3}\hat{\imath}),$$
$$\mathbf{K}_3=(4\pi/a\sqrt{3})\hat{\jmath}.$$

The volume of the BZ is

$$\Omega_K=\mathbf{K}_1\cdot\mathbf{K}_2\times\mathbf{K}_3=\frac{16\pi^3\sqrt{3}}{3a^2c}=\frac{8\pi^3}{\Omega_0}.$$

The radius of the free-electron Fermi sphere is defined by

$$\tfrac{4}{3}\pi k_0^3=2\Omega_K,$$

since with four conduction electrons per unit cell the volume of occupied states is equal to twice that of the BZ. This gives $k_0=1.027$.

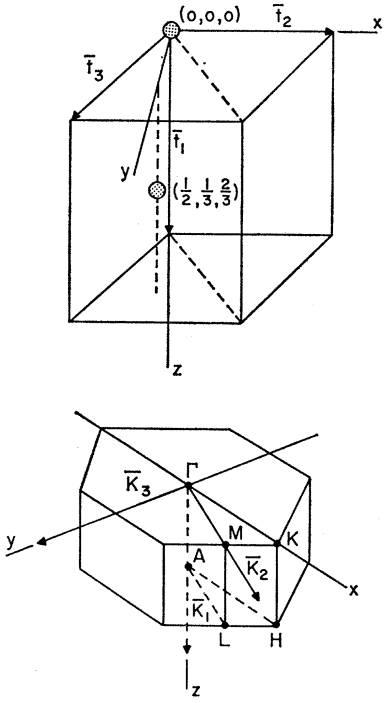

FIG. 1. Unit cell in hexagonal close-packed lattice showing locations of the two atoms; first Brillouin zone with 1/24th zone outlined by points of high symmetry $\Gamma KMLHA$.

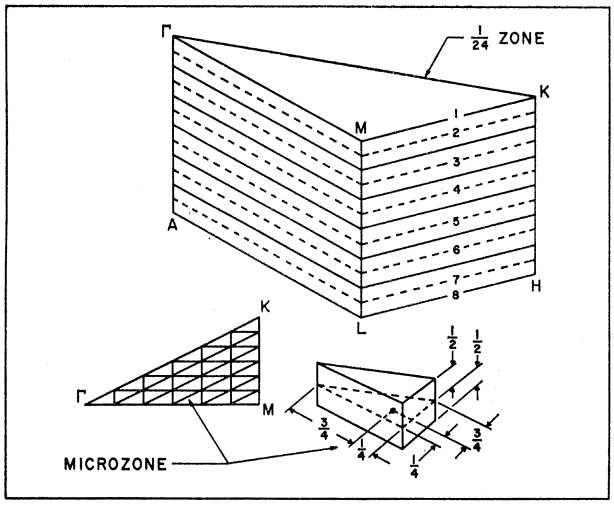

FIG. 2. Subdivision of 1/24th zone into 216 microzones and location of representative point.

Because of symmetry it is necessary to consider only 1/24th of the BZ. This 1/24th zone is outlined in Fig. 1 by the points of high symmetry $\Gamma KMAHL$. This zone was partitioned into 216 microzones by subdividing each of the sides into 6 equal parts. A point in the "center" of each of these triangular prisms was assigned to represent the states contained in the microzone (see Fig. 2). The BZ is thus represented by $216\times24=5184$ general points.

OPW Method

The theory of the OPW method has been reviewed frequently, with the most detailed discussion given by Woodruff.[4] Essentially it amounts to treating the coefficients of a truncated reciprocal lattice expansion of the wave function as variational parameters which are chosen such that the energy is minimized. The basis for the expansion is taken to be plane waves which have been orthogonalized to the core states. Dispensing with the details, the matrix elements of the secular determinant are given by

$$H_{ij}=\tfrac{1}{2}A_iA_j\zeta(\mathbf{G}_{ji})\{k_i^2\delta_{ij}+(8\pi/\Omega_0)\times[\lambda\Lambda(g;k_i)\Lambda(g;k_j)-\Lambda(h;G_{ji})]\},$$

$$\Delta_{ii}=1,$$

$$\Delta_{ij}=-(4\pi/\Omega_0)A_iA_j\zeta(\mathbf{G}_{ji})\Lambda(g;k_i)\Lambda(g;k_j),$$

where

$$\Lambda(t;x)=\int_0^\infty t(r)\frac{\sin(xr)}{x}dr,$$

$$\zeta(\mathbf{G}_{ji})=1+\exp[2\pi i(\tfrac{1}{2}j_1+\tfrac{1}{3}j_2+\tfrac{2}{3}j_3)],$$

$$\mathbf{G}_{ji}=\mathbf{G}_j-\mathbf{G}_i=[j_1,j_2,j_3],$$

$$\mathbf{k}_i=\mathbf{k}+\mathbf{G}_i,$$

$$A_i=[1-(8\pi/\Omega_0)\Lambda^2(g;k_i)]^{-1/2}.$$

[9] D. R. Schwarzenberger, Phil. Mag. 4, 1242 (1959).

$\mathbf{k}$ is the wave vector of the electron and $\mathbf{G}_j$ is a reciprocal lattice vector $[l,m,n]$, where l, m, n are integers. $g(r)$ is defined by

$$\psi(r)=(4\pi)^{-1/2}g(r)/r,$$

where $\psi(r)$ is the normalized core wave function. When the total potential is written as the sum of atomic-like potentials centered on the lattice sites,

$$U(r)=\sum_{\text{lattice}} V(|\mathbf{r}-\mathbf{R}_\alpha|),$$

then $h(r)$ is defined by

$$h(r)=-rV(r).$$

λ is the absolute value of the core eigenvalue, i.e., solutions of Schrödinger's equation for the potential $V(r)$. The conduction state eigenvalues are determined by finding those values of E such that

$$|H_{ij}-E\Delta_{ij}|=0.$$

Potential

As mentioned in the Introduction, the potential constructed for this band calculation is felt to be reasonably self-consistent. Explicitly, to the extent that the conduction electrons can be represented by a spherically symmetric single OPW and that core electrons are represented by the ground-state solution of Schrödinger's equation using the atomic-like potential $V(r)$, and to this extent only, is the potential self-consistent. Limited as this framework might be it is a step in the right direction. The remaining step must bring in dependence on $\mathbf{k}$ and ultimately dependence on the band. This, of course, is out of the question today. It should be mentioned, however, that an attempt was made to make the potential $|\mathbf{k}|$-dependent. To do this the momentum range between zero and k_0 was divided into eight equal intervals. In the exchange terms (conduction-core and conduction-conduction) the k dependence was retained and eight different potentials were constructed. As the conduction eigenvalues were being determined for an arbitrary point in the BZ, the magnitude of $\mathbf{k}$ was used to call in the appropriate potential curve. The difficulty with this procedure was that the energy bands had discontinuities at the points where a change between potential curves was made. Eight division were not sufficient to smoothly represent the k dependence. One could, of course, smooth these steps out in an arbitrary fashion or even take more than eight divisions, but it was felt that the additional complication was not warranted at the present. The change to an average value of k produced only small changes in the potential.

To construct a self-consistent potential one would probably treat the conduction electrons as plane waves and the core electrons as those in the free atom. However for beryllium the first iteration had already been performed by Pomerantz and Das.[10] In calculating the field gradient at the nucleus they constructed a potential with the following terms:

(1) Core Coulombic potential due to the charge Z on the nucleus and $1s$ electrons taken to be the same as for the neutral Be atom.[11]

(2) Core-conduction exchange potential due to a weighted mean between a $2s$ electron in the $1s^22s^2$ configuration and a $2p_z$ electron in the $1s^22p_z^2$ configuration.

(3) Conduction Coulombic potential due to two electrons in the Wigner-Seitz sphere in single OPW states (constructed using Be atom core states and free-electron conduction states).

The core-conduction exchange bumps were then smoothed out, and the resulting potential was used to calculate a new single OPW charge density for the conduction states. Using this final potential (see Fig. 3 in Ref. 10) we repeated the last stage of their calculations as a check and began from this point the iterations toward a self-consistent potential.

The various contributions which were considered in the construction of the self-consistent potential were:

$h_a(r)$—potential due to the ion-core,
$h_b(r)$—correlation among core electrons,
$h_c(r)$—exchange between conduction and core electrons,
$h_d(r)$—potential due to the conduction electrons,
$h_e(r)$—potential due to deviation from spherical symmetry,
$h_f(r)$—exchange and correlation among conduction electrons.

Each of these will now be discussed in some detail.

We begin with the ordinary Coulombic potential due to the positive charge $Z=4$ on the nucleus; the other contribution to the ion-core potential comes from the core electrons. Once the core wave functions are known, the potential follows from Poisson's equation. To get the wave functions Schrödinger's equation was integrated numerically using the computed form of the self-consistent potential. These two numerical procedures are by now quite standard and will not be discussed here.[12] The final core wave function is shown in Fig. 3. It is interesting that it is nearly identical to the $1s$ wave function for neutral beryllium as determined by Roothan, Sachs, and Weiss[13] using a generalized self-consistent field (SCF) formalism. The most sensitive parameter in the iteration procedure for the

[10] M. Pomerantz and T. P. Das, Phys. Rev. **119**, 70 (1960).
[11] P. M. Morse, L. A. Young, and E. S. Haurwitz, Phys. Rev. 48, 948 (1935).
[12] For details in numerical procedures see T. L. Loucks, Ph.D. thesis, The Pennsylvania State University, 1963 (unpublished).
[13] C. C. J. Roothan, L. M. Sachs, and A. W. Weiss, Rev. Mod. Phys. **32**, 186 (1960).

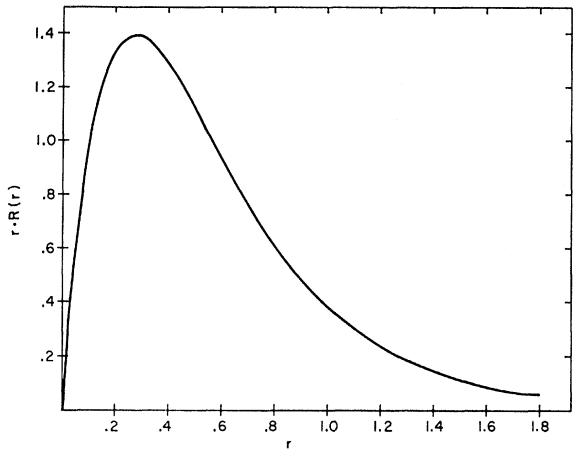

FIG. 3. Radial part of core wave function in self-consistent potential.

potential was λ. Therefore, it was used to determine the extent to which self-consistency had been obtained. The values at different stages of the iteration are shown in Table I. The starting and final values of this contribution to the total potential are shown in Fig. 4. The change resulting from the potential iteration is not large. The principal effect has been to establish a stabilized self-consistent value of λ. This is important because of the sensitivity of the OPW matrix elements to this parameter. The numerical values of the final ion-core potential are listed as $h_a(r)$ in Table II.

Correlation energy between core electrons as calculated in the present work is a very small contribution to the total potential. Correlation between core electrons was assumed to be the same as that between the two electrons in doubly ionized beryllium. It was decided to use the Be^{++} wave functions computed by Löwdin and Rédei[14] which include correlation by assuming a wave function of the form

$$\psi(r_1,r_2)=u(r_1)u(r_2)(1+\alpha r_{12}),$$

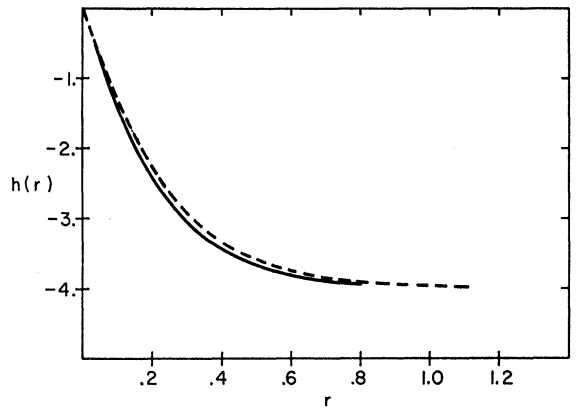

FIG. 4. Coulombic potential of core electrons: dashed line first iteration, solid line self-consistent potential.

[14] P. O. Lowdin and L. Redei, Phys. Rev. **114**, 752 (1959).

where

$$u(r)=(4\pi)^{-1/2}(A_1e^{-a_1r}+A_2e^{-a_2r}).$$

The one-electron charge density was found by integrating $\psi^2(r_1,r_2)$ over the coordinates of one of the electrons. The difference between the resulting charge density and that given by the self-consistent field type calculation was used in Poisson's equation to determine the potential due to correlation. The three parameter empirical formula given by Green, Mulder, Lewis, and Woll[15] was used for the SCF solution. This contribution is listed as $h_b(r)$ in Table II. It was taken to be the same at each stage of the potential iteration.

Exchange between core and conduction electrons was treated by evaluating the exchange integral to second order in spherical harmonic expansions. The potential is given by

$$V_{ex}(x,k)=-2\left\langle\frac{\psi_{1s}(x)}{\psi_{OPW}(\mathbf{x},\mathbf{k})}\int\frac{\psi_{1s}(t)\psi_{OPW}(\mathbf{t},\mathbf{k})d^3t}{|\mathbf{x}-\mathbf{t}|}\right\rangle,$$

where the angular brackets indicate an average over the angle between $\mathbf{x}$ and $\mathbf{k}$. ψ_{1s} is the numerically tabulated core wave function from the most recent stage in the potential iteration. ψ_{OPW} takes the usual form

$$\psi_{OPW}(\mathbf{t},\mathbf{k})=(2/\Omega_0)^{1/2}\exp(i\mathbf{k}\cdot\mathbf{t})-B_k\psi_{1s}(t),$$

where the B_k are the orthogonalization coefficients

$$B_k=(8\pi/\Omega_0)^{1/2}\Lambda(g;k).$$

In the evaluation of the exchange integral the spherical harmonic expansion for $(|\mathbf{x}-\mathbf{t}|)^{-1}$ and Bauer's formula for the exponential term were used. Only the first two terms in the resulting expansion were retained since a calculation showed that in the range of interest the second-order contribution was always less than $\frac{1}{4}$th the first-order term. The OPW wave function in the denominator was then expressed as a sum of real and imaginary parts; the final result can be summarized as follows:

$$V_{ex}(x,k)=\int_0^\pi \sin\beta V_{ex}(x,k,\beta)d\beta,$$

$$V_{ex}(x,k,\beta)=-2\psi_{1s}(x)\frac{V_R\psi_R+V_I\psi_I}{\psi_R^2+\psi_I^2},$$

$$V_R=(2/\Omega_0)^{1/2}S_0-B_kf(x),$$

$$V_I=(2/\Omega_0)S_1,$$

$$\psi_R=(2/\Omega_0)^{1/2}\cos(xk\cos\beta)-B_k\psi_{1s}(x),$$

$$\psi_I=(2/\Omega_0)^{1/2}\sin(xk\cos\beta),$$

$$S_0=\frac{4\pi}{x}\int_0^x\psi_{1s}(t)\left(\frac{\sin kt}{k}\right)tdt+4\pi\int_x^\infty\psi_{1s}(t)\left(\frac{\sin kt}{k}\right)dt,$$

[15] L. Green, M. Mulder, M. Lewis, and J. Woll, Phys. Rev. **93**, 757 (1954).

$$S_1=\frac{4\pi\cos\beta}{x^2}\int_0^x \psi_{1s}(t)\left(\frac{\sin kt-kt\cos kt}{k^2}\right)tdt$$

$$+4\pi x\cos\beta\int_x^\infty \psi_{1s}(t)\left(\frac{\sin kt-kt\cos kt}{k^2t^2}\right)dt,$$

$$f(x)=\int\frac{\psi_{1s}^2(t)d^3t}{|\mathbf{x}-\mathbf{t}|}.$$

$f(x)$ was found by solving Poisson's equation

$$\nabla^2 f=-4\pi\psi_{1s}^2.$$

$V_{ex}(x,k)$ was evaluated using $k=\frac{3}{4}k_0$ as an average value. The results for $h_c(r)=-rV_{ex}(r)$ are shown in Fig. 5 and the final self-consistent results are tabulated in Table II.

TABLE I. Core-state eigenvalues in the crystal potential at different stages of the iteration.

Stage of iteration	Core-electron eigenvalue (arbitrary zero of energy)
First	−5.4387
Second	−7.0497
Third	−6.7648
Fourth	−6.7653

The Coulombic potential due to the conduction electrons was calculated using the charge density

$$\rho(r)=\frac{\Omega_0}{8\pi^3}\int|\psi(\mathbf{k},\mathbf{r})|^2d^3k$$

in Poisson's equation. Here the integration was taken

TABLE II. The self-consistent crystal potential.

r	$h_a(r)$	$h_b(r)$	$h_c(r)$	$h_d(r)$	$h_e(r)$	$h_f(r)$	Total $h(r)$
0.00	8.000	0.000	0.000	0.000	0.000	0.000	8.000
0.04	7.422	−0.054	0.168	−0.109	0.006	0.043	7.476
0.08	6.883	−0.081	0.326	−0.216	0.012	0.071	6.995
0.12	6.399	−0.091	0.467	−0.320	0.018	0.087	6.560
0.16	5.978	−0.092	0.589	−0.421	0.024	0.093	6.170
0.20	5.618	−0.087	0.694	−0.520	0.030	0.090	5.824
0.24	5.315	−0.080	0.786	−0.615	0.036	0.080	5.520
0.28	5.063	−0.072	0.871	−0.710	0.042	0.062	5.256
0.32	4.855	−0.063	0.955	−0.802	0.048	0.039	5.031
0.36	4.685	−0.055	1.048	−0.894	0.053	0.011	4.849
0.40	4.548	−0.047	1.163	−0.985	0.059	−0.022	4.717
0.44	4.437	−0.040	1.318	−1.075	0.065	−0.059	4.646
0.48	4.347	−0.034	1.533	−1.165	0.071	−0.098	4.654
0.52	4.276	−0.028	1.821	−1.256	0.077	−0.135	4.755
0.56	4.220	−0.024	0.620	−1.346	0.083	−0.159	3.395
0.60	4.175	−0.020	−0.658	−1.435	0.089	−0.160	1.991
0.64	4.139	−0.016	−0.443	−1.525	0.095	−0.150	2.100
0.68	4.110	−0.013	−0.301	−1.615	0.101	−0.137	2.144
0.72	4.088	−0.011	−0.208	−1.705	0.107	−0.125	2.146
0.76	4.069	−0.009	−0.145	−1.794	0.113	−0.113	2.122
0.80	4.055	−0.007	−0.102	−1.883	0.119	−0.102	2.080
0.84	4.044	−0.006	−0.072	−1.971	0.125	−0.092	2.028
0.88	4.035	−0.005	−0.050	−2.059	0.131	−0.083	1.969
0.92	4.027	−0.004	−0.035	−2.146	0.137	−0.075	1.905
0.96	4.022	−0.003	−0.024	−2.232	0.143	−0.068	1.838
1.00	4.017	−0.002	−0.016	−2.317	0.149	−0.061	1.769
1.08	4.011	−0.001	−0.006	−2.485	0.160	−0.049	1.629
1.16	4.006	−0.001	−0.001	−2.647	0.172	−0.040	1.490
1.24	4.004	−0.001	0.001	−2.803	0.184	−0.032	1.354
1.32	4.002	0.000	0.002	−2.953	0.196	−0.026	1.222
1.40	4.001	0.000	0.002	−3.095	0.208	−0.020	1.096
1.48	4.001	0.000	0.002	−3.230	0.220	−0.016	0.977
1.56	4.000	0.000	0.002	−3.355	0.232	−0.013	0.866
1.64	4.000	0.000	0.002	−3.472	0.244	−0.010	0.764
1.72	4.000	0.000	0.001	−3.578	0.255	−0.008	0.671
1.80	4.000	0.000	0.001	−3.674	0.267	−0.006	0.589
1.88	4.000	0.000	0.001	−3.758	0.279	−0.005	0.517
1.96	4.000	0.000	0.001	−3.830	0.291	−0.004	0.457
2.04	4.000	0.000	0.000	−3.892	0.303	−0.003	0.409
2.10	4.000	0.000	0.000	−3.929	0.312	−0.002	0.382
2.20	4.000	0.000	0.000	−3.974	0.304	−0.001	0.329
2.30	4.000	0.000	0.000	−3.997	0.256	0.000	0.258
2.40	4.000	0.000	0.000	−4.000	0.203	0.000	0.203
2.50	4.000	0.000	0.000	−4.000	0.148	0.000	0.148
2.60	4.000	0.000	0.000	−4.000	0.150	0.000	0.150
2.70	4.000	0.000	0.000	−4.000	0.127	0.000	0.127
2.80	4.000	0.000	0.000	−4.000	0.090	0.000	0.090
2.90	4.000	0.000	0.000	−4.000	0.050	0.000	0.050
3.02	4.000	0.000	0.000	−4.000	0.000	0.000	0.000

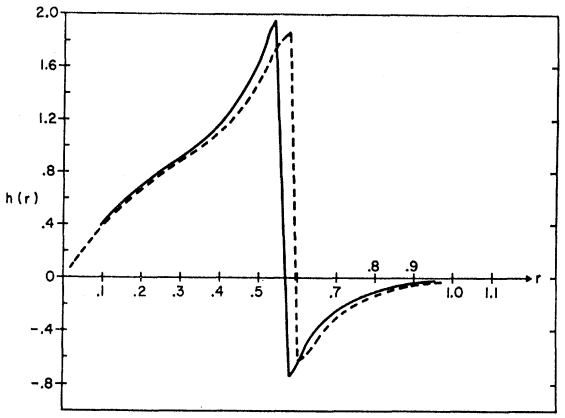

FIG. 5. Exchange potential between core and conduction electrons: dashed line first iteration, solid line self-consistent potential.

over the spherical Fermi surface of radius k_0, the wave function being a single OPW

$$\rho(r)=\frac{\Omega_0}{2\pi^2}\int_0^{k_0} A_k{}^2k^2dk\left\{\frac{2}{\Omega_0}+B_k{}^2\psi_{1s}{}^2(r) -2\left(\frac{2}{\Omega_0}\right)^{1/2}B_k\psi_{1s}(r)\frac{\sin kr}{kr}\right\}.$$

At each stage of the iteration this integration was performed numerically using the current values of A_k, B_k and ψ_{1s}. The resulting potential differed only slightly with each stage of the iteration, and the final result was essentially the same given by assuming an uniform distribution of electrons. Hence using OPW's did not effect this contribution to the crystal potential. The final charge density for the conduction electrons is shown in Fig. 6. The dip due to orthogonalization with the core state does not greatly affect the potential because it occurs near the origin and occupies such a small fraction of the total charge distribution. The final contribution of the conduction electrons to the total potential is listed as $h_d(r)$ in Table II.

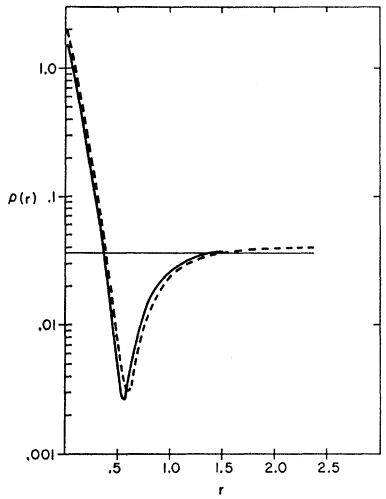

FIG. 6. Conduction electron charge density: dashed line first iteration, solid line self-consistent charge density.

The potential due to deviation from spherical symmetry has been treated in detail by both Heine and Falicov. Briefly, it is the potential due to the difference between two charge densities: (i) the charge density due to a lattice of protons and a uniform background of electrons; (ii) the charge density due to Wigner-Seitz spheres of electrons centered on the positive lattice sites. The uniform spheres of charge overlap in some regions while failing to cover others at all. By performing an Ewald-type sum at various points between the lattice sites one can develop a potential which takes account of the actual crystal lattice. The resulting correction term is listed as $h_e(r)$ in Table II. It is a small correction except in the region between the lattice sites where it has the effect of making the potential more binding. This contribution was kept constant during the potential iteration.

The final contribution to the crystal potential is that due to exchange and correlation among the conduction electrons. These two effects were included together by using a screened $\rho^{1/3}$ exchange. The justification of this follows from treating the electron density as a variable in the Pines expression for the average exchange energy per electron.[16] The result takes the form

$$V(r)=-6\left(\frac{3\rho(r)}{8\pi}\right)^{1/3}\left(1-\tfrac{4}{3}\beta+\frac{\beta^2}{2}-\frac{\beta^4}{48}\right),$$

where $\rho(r)$ is the conduction charge density discussed above. When β is determined by minimizing the long-range correlation energy it is given by

$$\beta=\alpha r_e{}^{1/2},$$

where $\alpha=0.35$ and the electronic radius, r_e, is defined by

$$\tfrac{4}{3}\pi r_e{}^3=\Omega_0/4.$$

If the electron-plasmon interaction is taken into account, then the value of α is 0.40. One can show by quantum-mechanical considerations that the upper bound to the value of α is 0.47. Thus, there seems to be some arbitrariness in the selection of β, but for this part of the calculation it was decided to use $\alpha=0.35$ which gives $\beta=0.482$. This choice of β agrees with the value obtained from characteristic energy loss measurements on thin films of beryllium. Since energy is measured from an arbitrary origin, the screened exchange potential was shifted so that it was zero in the region between the lattice sites where the charge density is uniform. The contribution to the total potential is listed as $h_f(r)$ in Table II.

There was a certain reluctance to use the screened $\rho^{1/3}$ exchange potential because of its known approximate form. An attempt was made to calculate the exchange between single OPW wave functions using

[16] D. Pines, Phys. Rev. 92, 626 (1953).

an exponential screening factor in the exchange integral. An expansion to second order in spherical harmonics was again used, as in the exchange integral between core and conduction electrons. However, the expressions were much more complicated, and the running time on the computer for a single value of the radius vector was far out of proportion to the improvement this approach could be expected to make. However, the values for small r were found using $k=\frac{3}{4}k_0$, and they were about half as large near the origin as those given by the screened $\rho^{1/3}$. These results differed further in that instead of a single dip, as appears in $\rho(r)$, there was a dip and a bump, much as in the case of core-conduction exchange.

A k-dependent exchange and correlation between conduction electrons was tried initially using the Bohm-Pines (BP) one-electron correlation formula for the free-electron gas. This procedure was used by Heine on aluminum and Falicov on magnesium, so the equations will not be repeated here [see Eq. (2.14), Falicov[6]]. In the computation, β was the same as in the screened $\rho^{1/3}$ expression. The use of the BP k-dependent exchange-correlation energy in this manner did not, however, give a correct Fermi surface for beryllium. The surface that resulted using the k-dependent BP term and $\beta=0.482$ consisted of: (i) a hole region in the first double zone which resembled a 3-toothed gear mounted in the center of an axle which is larger in the middle and tapers to rounded ends, (ii) a pocket of electrons similar to two milk saucers, one inverted on the other, and (iii) six identical little pockets of electrons with the shape and relative size of a cashew nut. At first it was thought that this surface, although quite different from the free-electron model, might yield the experimental de Haas-van Alphen frequencies. This was not found to be the case. By neglecting the Pines k-dependent screened exchange the resulting Fermi surface was found to be in very good agreement with all known experiments. This is really the only defense offered for this procedure.

The last column of Table II is the total crystal potential which was used to determine the OPW expansion matrix elements. These results are shown in Fig. 7 along with the potential used by other investigators. The potential used by Jacques[17] is not shown since it is essentially the same as that of HH.

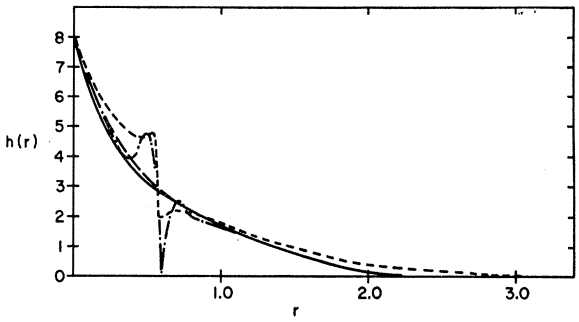

FIG. 7. Crystal potential: small dashed curve is the present work, dot-dash curve that of Pomerantz and Das before smoothing, large dashes Pomerantz and Das after smoothing and solid line the results of Herring and Hill.

Calculation of Energy Eigenvalues

The computer program for generating the energy eigenvalues begins by reading the coordinates of a point in k space. It then constructs four 23rd-order matrices: the real and imaginary parts of both the Hamiltonian and overlap matrices as described in the section on the OPW method. The same 23 reciprocal lattice vectors (those closest to the origin) were used for all points in the 1/24th zone. This process took about 50 sec on the IBM 7074. The next step is finding the lowest roots of the secular determinant. The method employed for this was simply to examine the determinant as a function of E and find the places at which it crossed the axis. This was a very efficient procedure when the roots were nondegenerate and well separated since one could then take fairly large steps throughout the region of interest and, once a change in sign was detected, zero in on the root by the method of false position. This approach became impractical, however, when the roots were close together or degenerate. For steps small enough to detect the roots there was a great deal of wasted computation in the regions away from the roots. Hence for those points which yielded no roots using a reasonable step size, it was necessary to resort to plotting the determinant and finding the approximate location of the roots graphically. It was then practical to scan through this limited region with a small enough scanning step to be able to locate the crossing of the axis. If two roots are truly doubly degenerate the determinant would be tangent to the axis and would not change sign. It turned out, however, that either due to numerical approximations or because not enough OPW's were taken in the expansion, all of the roots which are known to be degenerate from group theory were actually two roots very close together. Hence in practice it was possible to detect them by testing for a change in sign.

The above procedure requires an enormous amount of computation because of the numerous times that the determinant of a 23rd-order complex (Hermitian) matrix must be evaluated. These determinants were solved in the usual way of getting all zeros under the diagonal elements by adding and subtracting multiples of the rows to one another. The determinant of the resulting triangular matrix is simply the product of the diagonal elements. If the original matrix elements are $d_{\mu\nu}$ then the matrix elements of the desired triangular matrix can be written

$$D_{\mu\nu}=d_{\mu\nu}-\sum_{i=1}^{I-1}\frac{D_{\mu i}D_{i\nu}}{D_{ii}},$$

[17] R. Jacques, Cahiers Phys. **70, 71, 72** (1956).

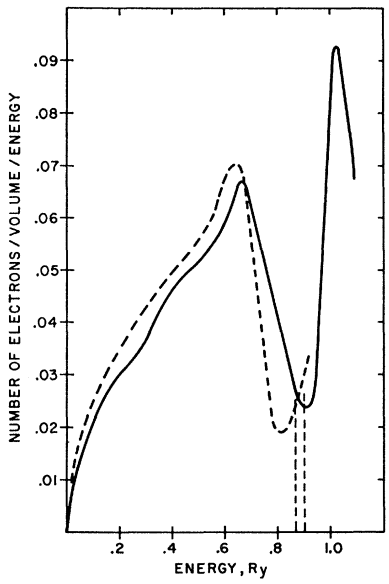

FIG. 8. Density of states $g(E)$: solid line is the result of the present computation and the dashed line is that of Herring and Hill. The Fermi energy is indicated by vertical dashed lines.

where I is the smaller of μ and ν. For starting values one takes $D_{1\nu}=d_{1\nu}$ and $D_{\nu 1}=d_{\nu 1}$ for $\nu=1, 2, \cdots, 23$. Then the determinant is simply $\prod_i D_{ii}$. This procedure was programmed for complex matrix elements and required 3 or 4 sec execute time for the evaluation of one 23rd-order determinant.

RESULTS

Fermi Energy

Since the 1/24th zone was divided into 216 microzones and since the volume of occupied states is equal to twice that of the BZ, then if all the energy eigenvalues computed at the general points are placed in ascending order the Fermi energy must be the 432nd eigenvalue. All the energies less than (and equal) to this value are occupied and all those above are empty at the zero of absolute temperature. This value was found to be

$$E_f=0.901 \text{ Ry}$$

as measured from the bottom of the band. In this, and in all other results unless specified differently, a reference to energy will mean the values obtained from the potential given in Fig. 7 without any correction for k-dependent exchange. This was discussed in the section on Potential.

Density of States

Having ordered the eigenvalues to obtain the Fermi energy it is a straight forward calculation to get the density of states $g(E)$. This function was normalized so that the area representing occupied states would be equal to the number of electrons per unit volume. Since there are two electrons per atom and two atoms per unit cell, we obtain

$$\int_0^{E_f} g(E)dE=\frac{4}{\Omega_0}.$$

The energy range was divided into increments ΔE and the number of energy levels in each increment, $M(E)$, determined. The density of states was then calculated using

$$g(E)=4M(E)/\Omega_0(2\times 216)\Delta E.$$

The values of $g(E)$ were plotted in the center of the energy increment which they represented. A smooth curve was then drawn through these points. This was done for $\Delta E=0.03, 0.04, \cdots, 0.10$. The curves are slightly different in each case because we are approximating a very dense distribution with only 216 points.

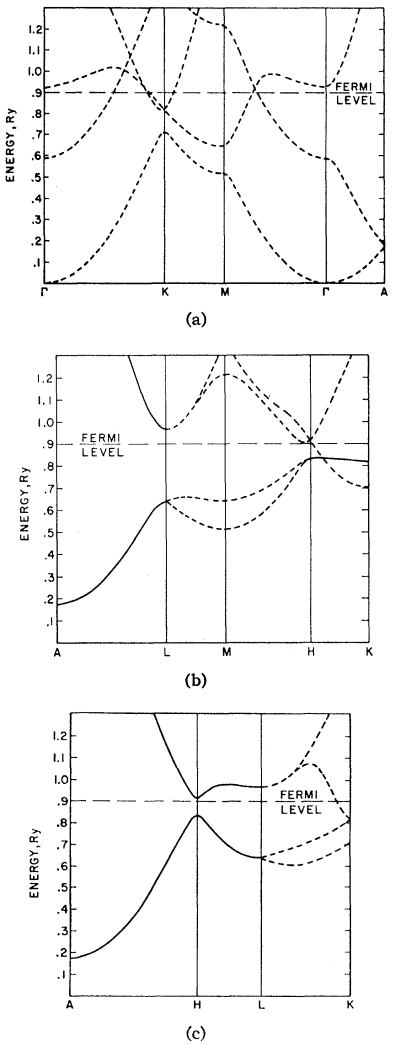

FIG. 9. Conduction electron energy eigenvalues: the dashed and solid lines denote nondegenerate and doubly degenerate bands, respectively.

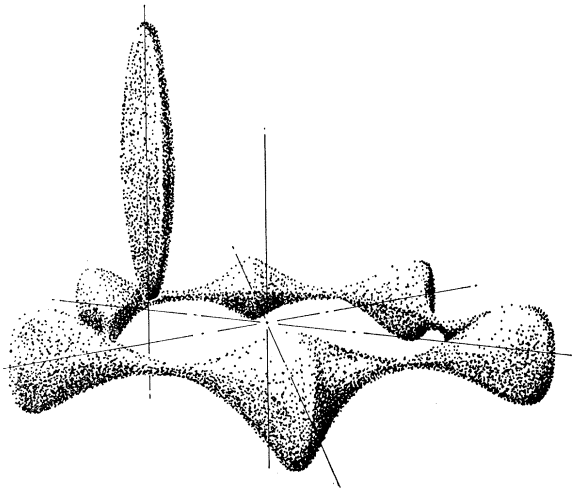

FIG. 10. The Fermi surface: cigar and coronet.

If ΔE is taken to be too small there are so few energy levels in each increment that the procedure is statistically unsound. On the other hand, if ΔE is taken to be too large there are only a few points to define the density-of-states curve and all the detail is lost. By examining all of the curves it was decided that $\Delta E = 0.07$ was the best for this case. The resulting density-of-states curve is shown in Fig. 8 with the Fermi energy as determined above.

Energy Bands and Fermi Surface

The energy bands along the symmetry edges are shown in Fig. 9. Similar plots of the bands along the edges of the microzones were also made. By determining the intersections of the bands with the Fermi energy along all of these traverses of the 1/24th zone it was possible to define quite accurately the Fermi surface. There are three pieces of the Fermi surface: a region of holes or unoccupied states in the first double zone and two identical pockets of electrons in the second double zone. These pieces of the surface are shown pictorially in Fig. 10. Cross sections of the Fermi surface are shown in Fig. 11. The numbers on the contours correspond to the planes through the 1/24th zone as indicated in Fig. 2. The intersection of the Fermi surface with the zone faces is shown in Fig. 12.

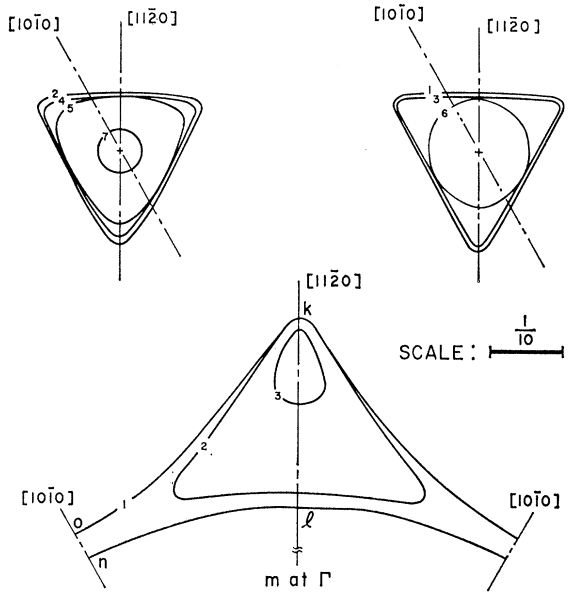

FIG. 11. Cross sections of the Fermi surface along planes numbered according to Fig. 2.

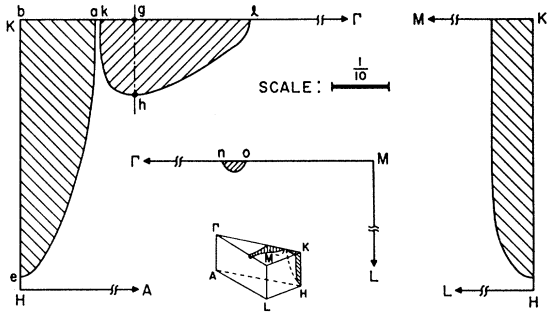

FIG. 12. Intersections of Fermi surface with 1/24th zone faces.

DISCUSSION OF RESULTS AND COMPARISON WITH EXPERIMENTS

Convergence

It is difficult to determine the extent to which the OPW expansion has converged. In Fig. 13 the lowest eigenvalues for Γ, K, and H, as measured from the bottom of the band, are shown for various expansions ranging from 3 to 23 OPW's. The Γ_3^+, K_1, and H_2 levels are changed very little by increasing the number of OPW's. The Γ_4^- level decreases between 5 and 9 OPW's but then remains the same. H_1 does not decrease until 19 OPW's are used but is constant, thereafter, to 23. The greatest change comes in the upper K_2 level.

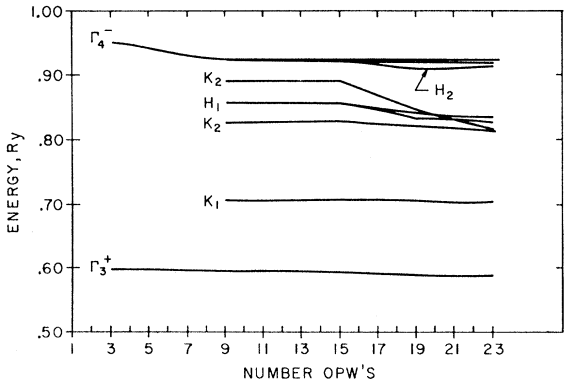

FIG. 13. Energy eigenvalues at three points of high symmetry as a function of the number of OPW's used in the conduction electron wave function expansion.

TABLE III. Summary of theoretical bandwidth determinations.

	Bandwidths (Ry)
Free electron	1.055
Herring and Hill[a]	0.865
Jacques:[b]	
Single OPW	0.956
OPW with variational parameter	0.919
APW method	0.840
Cornwell[c]	0.780
Present work	0.901
Skinner[d] (experimental)	1.01±0.07

[a] See Ref. 1.
[b] See Ref. 17.
[c] See Ref. 23.
[d] See Ref. 18.

K_2 is known to be a doubly degenerate level and the secular determinant should be tangent to the axis at the eigenvalue. This condition is very nearly satisfied only with the maximum number of 23 OPW's. The fact that the level does become degenerate as expected is felt to be a good indication that the levels have essentially converged with 23 OPW's.

Fermi Energy and Density of States

Various calculations of the bandwidth or Ferml energy have been listed in Table III. The experimental result given by Skinner[18] in 1946 is included for comparison. We have not attributed much importance to this comparison of our bandwidth with the experimental result because of the difficulties inherent in the extrapolation of the low-energy tail of the x-ray spectra.

The density-of-states curve of HH is shown in Fig. 8 along with our result. The experimental emission spectra as determined by Fisher, Crisp, and Williams[19] using a photon-counting, grazing incidence spectrometer is shown in Fig. 14. Their results are in most respects similar to those reported by other experimenters (see Yakowitz and Cuthill[20] for a bibliography on soft x-ray spectroscopy). The high-energy side of the spectrum

TABLE IV. Comparison of representative dimensions from the theoretical and experimental (Watts) Fermi surfaces.

Designation	Distance Theory	Distance Experiment
ml	0.57	0.57
lk	0.26	0.23
ka	0.01	0.08
ab	0.13	0.09
be	0.44	0.48
no	0.04	0.02
gh	0.13	0.12
mn	0.57	0.57

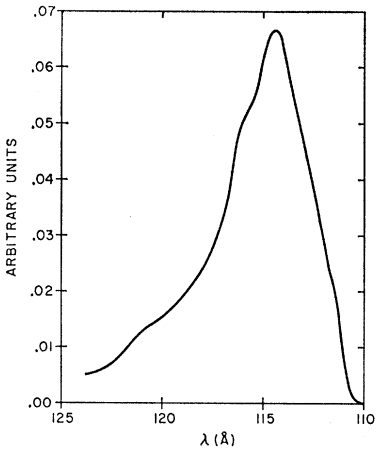

FIG. 14. Soft x-ray emission spectra of Fisher, Crisp, and Williams. Ordinate scale arbitrarily selected so that maximum coincides with theoretical results.

usually has a slope less abrupt than that caused by the sudden onset of vacant states above the Fermi energy. This is felt to confirm the dip in our theoretical density of states. There is, in fact, a kink in the experimental spectrum around 111.4 Å which could very well be due to the Fermi energy occurring at the dip in the density of states. This is certainly consistent with our results. The results of HH predict a sharp increase in the spectrum just below the Fermi energy. This is not observed in any of the spectra listed in Yakowitz and Cuthill. On the low-energy side of the peak there are two dips in our density of states. These seem to be reflected also in the emission spectra (Fig. 14). A more recent measurement of the valence band emission spectra by Sagawa[21] also displays dips similar to these, but they are attributed to Si $L_{II,III}$ absorption because of the glass grating used. Hence there is some question as to whether these dips would appear in the experimental results after corrections were made for this anomaly.

An additional feature of the density-of-states curve is felt to be confirmed by the experimental results of Johnston and Tomboulian.[22] They have shown that the absorption edge coincides with the high-energy limit of the emission line. This confirms that there is no forbidden zone in the density of states (i.e., beryllium is an electrical conductor). Further, the absorption data exhibits a sharp peak at the low-energy end which is consistent with the peak in the density of states just above the Fermi energy.

As a final comparison, the density of states at the Fermi energy was used to calculate the low-temperature specific heat coefficient. The result (for both our data and HH) was 0.54×10^{-4} cal/mole/deg^2 which is identical to the experimental result given by Hill and Smith. Cornwell[23] calculated 0.91×10^{-4} cal/mole/deg.^{2}

[18] H. W. B. Skinner, Phil. Trans. Roy. Soc. (London) **A239**, 95 (1946).
[19] P. Fisher, R. S. Crisp, and S. E. Williams, Opt. Acta **5**, 31 (1958).
[20] H. Yakowitz and J. R. Cuthill, Nat. Bur. Std. (U.S.) Monograph **52**, (1962).
[21] T. Sagawa, Sci. Rept. Tohoku Univ., First Ser. **45**, 232 (1961).
[22] R. W. Johnston and D. H. Tomboulian, Phys. Rev. **94**, 1585 (1954).
[23] J. F. Cornwell, Proc. Roy. Soc. (London) **A261** 551 (1961).

TABLE V. Comparison of frequency in $1/H$ from de Haas-van Alphen measurements (Watts) and from the theoretical Fermi surface.

Orbit designation	Direction	Area	Frequency (10^6 G) Theory	Experiment
Cigars:	$[11\bar{2}0]$	0.141	52.9	53.
	10° from $[11\bar{2}0]$ to $[10\bar{1}0]$	0.146	54.6	53.
	20° from $[11\bar{2}0]$ to $[10\bar{1}0]$	0.147	55.0	53.
	$[10\bar{1}0]$	0.149	55.7	53.
	[0001]	0.0245	9.2	9.8
Coronet:				
Inner circle	[0001]	1.04	389.	396.
Outer path	[0001]	1.47	550.	not given
Neck	$[11\bar{2}0]$	0.0014	0.53	0.23
Neck	$[11\bar{2}0]$	0.0006	0.23	0.11
Neck	$[10\bar{1}0]$	0.0008	0.30	0.12
Belly	$[11\bar{2}0]$	0.038	14.2	12.5
Belly	$[11\bar{2}0]$	0.055	20.7	15.0

Fermi Surface

The Fermi surface consists of three pieces; we will use the monarchial terminology of Watts[8] and describe the hole region in the first double zone as a coronet and the electron pockets in the second double zone as cigars (see Fig. 10). Watts deduced the Fermi surface from de Haas-van Alphen measurements. It differs from ours only in the following ways:

(1) Our cigars are not as long as Watts' and are triangular in cross section, becoming round only near the ends.

(2) Our coronet is slightly larger than Watts'.

The general agreement, however, is felt to be very good. Some extremal cross-sectional areas (A) were measured from our Fermi surface and the frequency in $1/H$ was calculated using the Onsager relation

$$f=\hbar cA/2\pi e.$$

These values are compared in Table V with the experimental frequencies given by Watts.

The two main differences listed above between our surface and that of Watts can be improved by raising the Fermi energy. However, this will still not make the cigars circular in cross section and will make them slightly too big around the waist. One could justly question our right to move the Fermi energy at all since it certainly is not arbitrary. However, it is possible that our method of determining the Fermi energy could be improved by selecting a more sufficiently representative set of points throughout the zone. This is supported by the fact that the volume of the hole region is somewhat bigger than that of the electron pockets. By raising the Fermi energy these volumes become equal. Further work in determining the Fermi energy such that the volume of the hole region is exactly equal to that of the electron pockets would be warranted. This work would involve more cross sections of the coronet than were done in this work. (Note added: Additional calculations have in fact already been carried out. The equivalent of 60 000 points in the BZ have been computed. It is found that electron and hole volumes are equal when

$$E_F=0.909,$$

thus raising the Fermi energy slightly.)

Changes in the potential as well as improvements in convergence of the OPW expansions could also contribute to the differences discussed above.

It should be mentioned that the energy bands of HH do not produce a coronet. The intersection of the bands between M and Γ occurs beneath their Fermi energy, and hence the necks of the coronet are severed leaving the bellies isolated. This model is anatomically inhumane as well as incorrect since it can not account for the observed λ oscillations in the [0001] direction.

ACKNOWLEDGMENTS

The authors wish to express their deepest gratitude to Dr. Leo M. Falicov of The University of Chicago for several stimulating conversations. We also acknowledge the cooperation of the staff at the Computation Center at The Pennsylvania State University.